

New Computer Assisted Diagnostic to Detect Alzheimer Disease

Ben Rabeah Amira

Signal, Information and Technology of Information (LR- SITI)
National Engineering School of Tunis (ENIT)
amira.benrabeh@gmail.com

Benzarti Faouzi

Signal, Information and Technology of Information (LR- SITI)
National Engineering School of Tunis (ENIT)
benzartif@yahoo.fr

Amiri Hamid

Signal, Information and Technology of Information (LR- SITI)
National Engineering School of Tunis (ENIT)
hamidlamiri@yahoo.fr

Mouna Ben Djebara

Alzheimer Service
Hospital Razi, Manouba, Tunis Tunisia
mounabdj@yahoo.fr

Abstract

We describe a new Computer Assisted Diagnosis (CAD) to automatically detect Alzheimer Patients (AD), Mild Cognitive Impairment (MCI) and elderly Controls, based on the segmentation and classification of the Hippocampus (H) and Corpus Calosum (CC) from Magnetic Resonance Images (MRI). For the segmentation we used a new method based on a deformable model to extract the area wishes, and then we computed the geometric and texture features. For the classification we proposed a new supervised method. We evaluated the accuracy of our method in a group of 25 patients with AD (age \pm standard-deviation (SD) =70 \pm 6 years), 25 patients with MCI (age \pm SD=65 \pm 8 years) and 25 elderly healthy controls (age \pm SD=60 \pm 8 years). For the AD patients we found an accuracy of the classification of 92%, for the MCI we found 88% and for the elderly patients we found 96%. Overall, we found our method to be 92% accurate. Our method can be a useful tool for diagnosing Alzheimer's Disease in any of these Steps.

Keywords: Computer Assisted Diagnosis (CAD), Alzheimer disease (AD), Mild Cognitive Impairment (MCI), Corpus Calosum (CC), Hippocampus (H), Magnetic Resonance Imaging (MRI), Standard Deviation (SD).

1. Introduction

Alzheimer's disease is the most common form of dementia among the elderly; it represents about 65% of dementia cases. Alzheimer's disease is distinguished from other dementias by the fact it develops gradually and it mainly affects the short-term memory. However, the diagnosis is not always easy and it can be difficult for physicians to differentiate Alzheimer's disease from another dementia (Weiner et al., 2015; Brumfield, 2014; Neville et al., 2015; Romero et al., 2014).

Generally, symptoms appear after 65 years and the prevalence increases sharply with age. However, contrary to popular belief, Alzheimer's disease is not a normal consequence of aging. Alzheimer's disease affects about 1% of people between 65 and 69 years old, 20% of those between 85 and 89 years old, and 40% of those between 90 and 95 years old (Mahad et al., 2015; Geerts et al., 2015; Kuffner et al., 2015). It is estimated that 1 in 8 men and 1 in 4 women will suffer from it in

their lives. Insofar as women live longer, they are more likely to be affected. We found several stages of Alzheimer's disease:

- MCI Mild Cognitive Impairment (memory loss which affects the short-term memory: the ability to remember recent information).
- the advanced stage (psychiatric problems, including hallucinations and paranoid delusions, aggravated by severe memory loss and disorientation) or what is called AD (Alzheimer's Disease) (Ruan et al., 2014; Cummings et al., 2014). In susceptible individuals the involution of the brain tissue is most pronounced in the hippocampus, the Corpus Callosum and anterior frontal cortex. In subjects with moderately severe Alzheimer's disease, the involution key comes in addition to the bottom and side portions of the temporal cortex and the posterior part of the limbic convolution. The disease is becoming more common. It is estimated that within 20 years, the number of sufferers will double (Romero et al., 2015; Panza et al., 2014; Saykin et al., 2015; Collins et al., 2015; Hartley et al., 2014).

Hence the need for a computerized diagnostic system to detected Alzheimer's disease. The steps of a computer-assisted diagnostic system may be as follows:

- The preprocessing step which serves to improve the quality of the image before any handling.
- The segmentation step for detecting the studied lesion.
- The description step, which is intended to characterize lesions through mathematical formulations.
- The classification step and decision-making by using an appropriate classifier.

Beginning with the segmentation, it discusses the methods based on the deformable model. We speak of three class methods: Parametric, Statistical, and Geometric.

In general, a deformable model can be defined as a curve dipped in the image plane, in a particular position, and which successively deforms until it coincides with the boundary of the object to be detected (Aljabar et al., 2009; Atif et al., 2006; Ardekani et al., 2009; Delingette et al., 2001; Duvernoy et al., 2005).

Our literature review on deformable models led us to grouping them into three classes, based on the above criteria: parametric models (Andreopoulos et al., 2008; Babalola et al., 2009; Bascle et al., 1994), geometric (Caselles et al., 1997; Chan et al., 2001; Charmi et al., 2008 ; Chen et al., 2005; Chen et al., 2004; Chen et al., 2009) and statistics (Cohen et al., 1991; Cootes, 1994 ; Cootes, 1995; Cootes, 2001).

In our method, the interest is in the geometric model.

The level set methods (LSM), which are a digital tool to analyze shapes, introduced by Osher and Sethian (1988), became a theoretical and numerical structure increasingly used in image processing. Compared to the active contours, the LSM has the advantage of avoiding the difficulties of topological transformations. Indeed, the approached level set is able to handle complex topological changes, e.g. develop a simple outline for two separate contours, or, conversely, combine two separate contours to form one. The Level Set Framework has several methods such as:

- Caselles: geodesic approach (Caselles et al., 1997);
- Chan & Vese: approach similar regions (Chan et al, 2001);
- Lankton: approach inhomogeneous regions (Lankton et al, 2008).

Passing the classification stage, the purpose of the classification is to identify the classes that the objects from descriptive features (attributes, characteristics, etc.) belong to. There are basically two types of classification: supervised and unsupervised. This classification is also called "clustering" or "grouping". In this type of classification it is necessary to identify populations of a data set. Suppose one has a set of objects denoted by $X = \{x_1, x_2, \dots, x_N\}$, characterized by a set of

descriptors D , and the clustering goal is to find the groups they belong to, each object x being noted with $C = \{C_1, C_2, \dots, C_n\}$.

That is to determine a function denoted by Y_S that associates each element of X to one or more of C . It should be able to assign a new observation to a class. Among unsupervised most common methods there are two types of approaches: k-means and hierarchical classification.

In the context of supervised already available examples whose class is known and labeled, the data are associated with labeled classes $\Theta = \{q_1, q_2, \dots, q_n\}$. The objective is to learn how to use the rules of a learning model that predict a class of new observations which determine a function from descriptors (D) of the object q_i , that allows you to combines classes and assign a new observation to the available classes. At the end, there needs to be found a function that Y_s that associates each element of X to an element of Q . We then constructed a model to classify new data. Among the supervised methods are cited: the k-nearest neighbors (Cover et al., 1967), decision trees (Quinlan, 1986), neural networks, support vector machines (SVM) (Cortes et al., 1995) and Bayes classifiers. Whatever type of classification, one is faced with different problems. In the supervised case, a significant problem may be the lack of data to perform learning or availability of inadequate data, such uncertainty and imprecision preventing the construction of a correct model. For unsupervised classifications, the demarcation of borders between classes is not always straight forward and recognizable. Regardless of the type of classification, multi dimensional data, or the dependence of classification methods to the initial settings, such as the number of classes, can impose problems. In our case, we are interested in the supervised classifier.

In this context is our work: performing a diagnostic computer-aided system for detecting Alzheimer's disease. Like any diagnostic system, our system contains three parts: preprocessing, segmentation and classification. Initially, we will present a new segmentation method to segment the Hippocampus and Corpus Callosum regardless of the patient's condition.

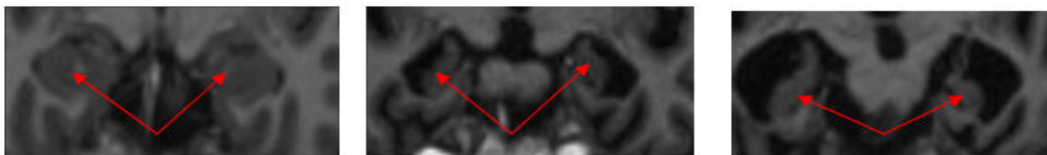


Figure 1. Three hippocampus: Normal, MCI, AD

The three figures above present three seahorses relating to three topics: Normal Subject, MCI Subject (Mild Cognitive Impairment), Alzheimer Subject.

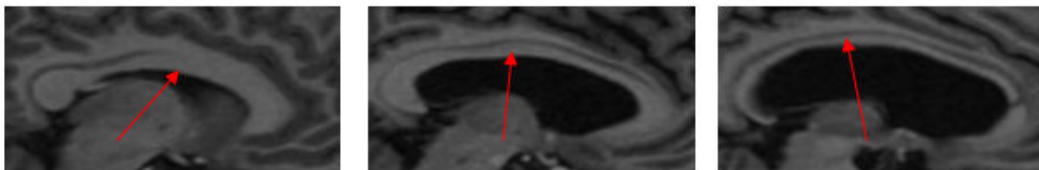


Figure 2. Three Corpus Calosum: Normal, MCI, AD

The three figures above present the Corpus Callosum relating to three topics: Normal Topic by MCI (Mild Cognitive Impairment), Alzheimer's topic.

Secondly, we will present our clustering method to classify the test subject between 3 classes: N (Normal), MCI (Mild Cognitive Impairment), and AD (Alzheimer's disease).

2. The proposed method

The figure below presents our proposed Computer Assisted Diagnosis. Our CAD includes 3 steps: Preprocessing, Segmentation and Classification.

For the step of preprocessing, we used the NLMS (Non Local Means) to improve the quality of image.

For the step of segmentation: we have a learning phase to extract the different shapes and to determine the average shape. Our proposed automatic method is based on the deformable model. For the step of classification, we present a new supervised method to distinguish between Normal, MCI and AD. The figure below presents our proposed system.

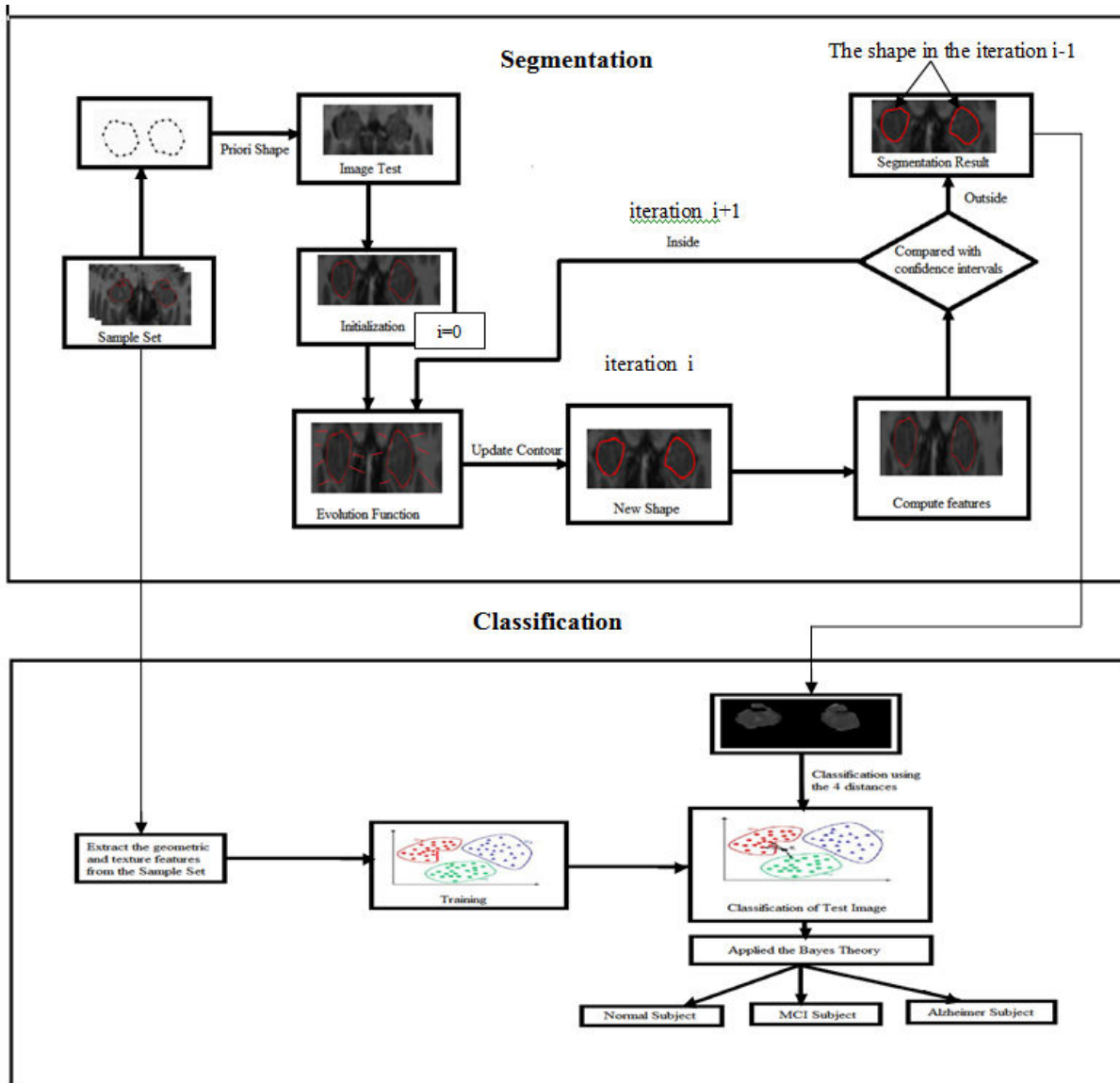


Figure 3. Proposed Computer Assisted Diagnosis

A. Segmentation

It seeks to establish a model that describes the shape and typical fluctuations. This requires first the preparation of a learning base to reflect the possible variations in shape of the structure.

The preparation of the training set

Each shape will be modeled by a vector X, built by concatenating the coordinates of the characteristic points placed on its outline:

$$X=(X1, X2, \dots, Xn) \quad (1)$$

The training set can be modeled by a set of vectors:

{X_i} Where i = 1 . . N {N number of sample images}

and {S_i} surface, {V_i} standard deviation of the Area.

The principle of this step is be illustrated by the figure below.

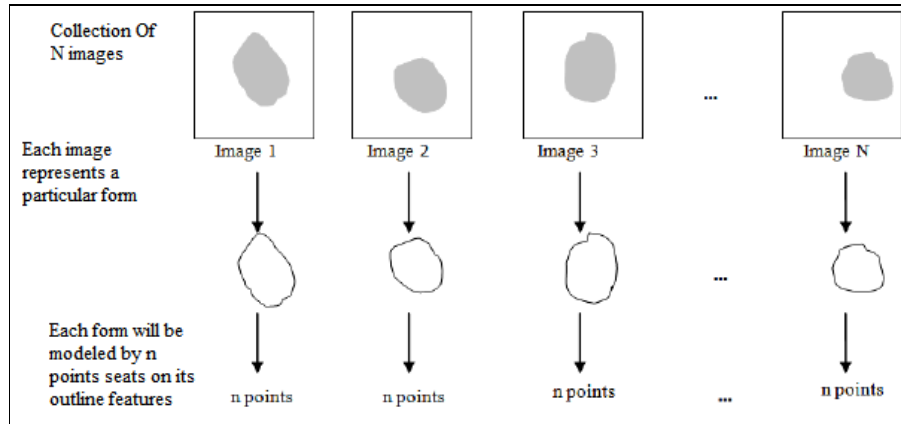


Figure 4. Training

Aligning the forms

During the previous step the extraction forms is independent on the parameters of size and position. They may have shapes which are more or less remote in different directions, and others that have relatively different sizes. However, the modeling approach is to study only the essential shape variation between the different configurations of the studied structure in order to solve this problem of variation of size and position. The N forms of the training set must be aligned with one of them. This will place the corresponding vector in a centered position.

Generating the average shape and confidence intervals

The aligned vectors, resultant of the two previous stages, can be organized in the form of a matrix of size (2n, N), called observation matrix. The columns match the shapes and the lines correspond to the coordinates of the points features describing each form.

$$\bar{x} = \frac{1}{N} \sum_{i=1}^N x_i \quad \text{The average shape from the training} \quad (2)$$

We also determine:

- the confidence interval associated with the area
 $[S_m - 2\sigma, S_m + 2\sigma]$ with (S_m average size, σ variation of the surface).
- the confidence interval associated with the surface
 $[V_m - 2\sigma, V_m + 2\sigma]$ with (V_m average variation, σ std of the variation).

The learning algorithm

Input:
 training set X (x_i, \dots, X_n)

Output:

1. Determine the initial parameters:
 - The number of images of the learning base: N
 - The number of minutiae: n
2. Extraction of forms $X_i = \{X_{i1}, X_{i2}, \dots, X_{in}\} \ i = 1 \dots N$
3. Aligning the learning database
4. Generation of average shape
5. Generation of confidence intervals associated with the surface and variation.
 - $[S_m - 2\sigma, S_m + 2\sigma]$ with (S_m average surface variation σ of the surface).
 - $[V_m - 2\sigma, V_m + 2\sigma]$ with (V_m average variation, σ std of the variation).

Evolution of the Curve

The stage in the evolution of the curve (loudness) is divided into two stages:

- designing a power function whose minimum corresponds to the contours of the object to segment;
- implementing the evolution equation.

Based on the work of Lankton, the objective is to outline converging towards locally homogeneous regions according to grayscale.

Energy minimization

$$E_{LAN}(\phi, U_{in}, U_{out}) = \iint_{\Omega} \delta(\phi(\vec{x})) \int B(\vec{x}, \vec{y}) F(\phi) \overline{dydx} \quad (3)$$

where (4)

$$F(\vec{x}, \vec{y}) = (I(\vec{y}) - U_{in}(\vec{x}))^2 H(\phi(\vec{y})) + (I(\vec{y}) - U_{out}(\vec{x})) H(-\phi(\vec{y}))$$

$$B(\vec{x}, \vec{y}) = \begin{cases} 1 & \text{with } \|\vec{x} - \vec{y}\| \leq r \\ 0 & \text{with } \|\vec{x} - \vec{y}\| > r \end{cases}$$

$$E(\phi, U_{in}, U_{out}) = \int_{\Omega} \delta(\phi(\vec{x})) \int B(\vec{x}, \vec{y}) F(\phi) \overline{dydx}$$

Select only the pixels belonging to the contour

$$E(\phi, U_{in}, U_{out}) = \int_{\Omega} \delta(\phi(\vec{x})) \int B(\vec{x}, \vec{y}) F(\phi) \overline{dydx}$$

Calculates the data attachment within a neighborhood centered at each point belonging to the contour

Equation of evolution outline:

$$\nabla_{\phi} E_{LAN} = \left(\int_{\Omega} B(\bar{x}, \bar{y}) \delta(\phi(\bar{y})) \nabla \phi F(\phi(\bar{y})) d\bar{y} \right) \delta(\phi(\bar{x})) \quad (5)$$

In the figures below a constraint of the variation is used in order to show the limits. The contour may include more areas surrounding the hippocampus, which are not homogeneous with the desired area. Through the confidence interval of variation and priori knowledge can overcome these limitations.

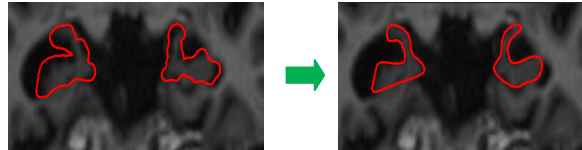


Figure 5. Improvement using variation

In the figures below, a constraint of the surface is used to show the limits. The contour may include the hippocampus and more areas surrounding it, which are homogeneous with the desired area. Through the surface of the confidence interval and priori knowledge can overcome these limitations.

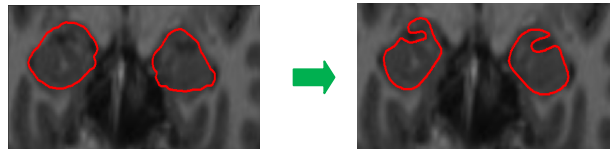


Figure 6. Improvement using Surface

The evolution algorithm

```

Input: Training set X (xi, ....., Xn)
       Picture Test
Output:
1. The mean shape is recovered
2. Retrieves confidence intervals associated with the surface and variation.
   - [Sm-2σ, Sm + 2σ] with (Sm average surface variation σ of the surface).
   - [Vm - 2σ, V m + 2σ] with (Vm average variation, σ std of the variation).
3. Function of evolution
   Stop = false
   While (stop ~ = true)
   { // Check that the surface of the next Fnew form is lower to the upper bound of the confidence
     interval for the same variation.
     If ((surface (Fnew) > Sm + 2σ) || (Variation (Fnew) > V m + 2σ))
       Stop = true;
     Else
       // Display the new form
       Converging towards the contour of the locally homogeneous regions according to the grayscale. }
    
```

B. Classification

The new method is a method of supervised classification. It has a learning database to estimate the output associated with a new entry X. The method takes into account the four training samples whose entrance is the closest to the new entry X in four distances: Euclidean, Manhattan, Hausdorff, AMED (Average Minimum Euclidean Distance).

The Euclidean distance

Given two vectors X (x1, x2... xn) and Y (y1, y2, ..., yn), different distances are expressed as follows:

Distance euclidienne:
$$\sum_{i=1}^n (x_i - y_i)^2 \tag{6}$$

Distance de Manhattan:
$$\sum_{i=1}^n |x_i - y_i| \tag{7}$$

The minimum Euclidean distance (MED) from x point x_i in X to Y is computed as:

$$MED(x_i, Y) = \min_{j \in \{1, \dots, n\}} \text{dist}(a_i, b_j) \tag{8}$$

Then the average minimum Euclidean distance (AMED) (Sahiner et al, 2001) and the Hausdorff distance (HD) (Huttenlocher et al, 1993) are defined as:

$$AMED(X, Y) = \frac{1}{2n} \sum_{i=1}^n MED(x_i, Y) + \frac{1}{2n} \sum_{j=1}^n MED(y_j, X) \tag{9}$$

and

$$HD(A, B) = \max \left\{ \max_{i \in \{1, \dots, n\}} MED(x_i, Y), \max_{j \in \{1, \dots, n\}} MED(y_j, X) \right\} \tag{10}$$

AMED measures the average distance while HD measures the maximum distance between the two vectors. The aim of our method is to classify the test subject in three classes (N, MCI or AD), so for each vector element E we look for the four nearest neighbors.

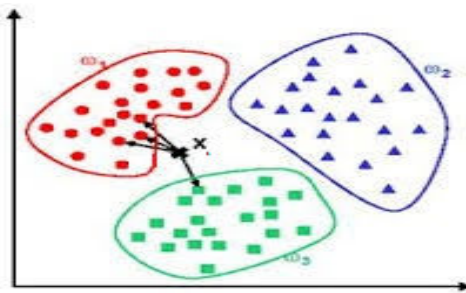


Figure 7. Training for classification

By using the four distances (Euclidean, Manhattan, Hausdorff, AMED - Average Minimum Euclidean Distance) 4 decisions are eventually obtained: A, B, C, D or A is the result of the test vector assignment to one of three classes using the first Euclidean distance.

To achieve the final result we use Bayes' theorem (Hooper, 2013).

The probabilistic model for a classifier is the conditional model

$$p(C | F_1, \dots, F_n) \quad (11)$$

Where C is a dependent class variable or a class whose instances are few, conditioned by several characteristic variables F_1, \dots, F_n .

When the number of characteristics is large, or when these features can take a large number of values, this model based on probability tables is impossible. Therefore, we derive to be more readily soluble. Using the Bayes' theorem, we write

$$p(C | F_1, \dots, F_n) = \frac{p(C) p(F_1, \dots, F_n | C)}{p(F_1, \dots, F_n)} \quad (12)$$

3. Results and discussion

The results show the hippocampus segmentation using both Caselle, Chan&Vese, Lankton and our method.

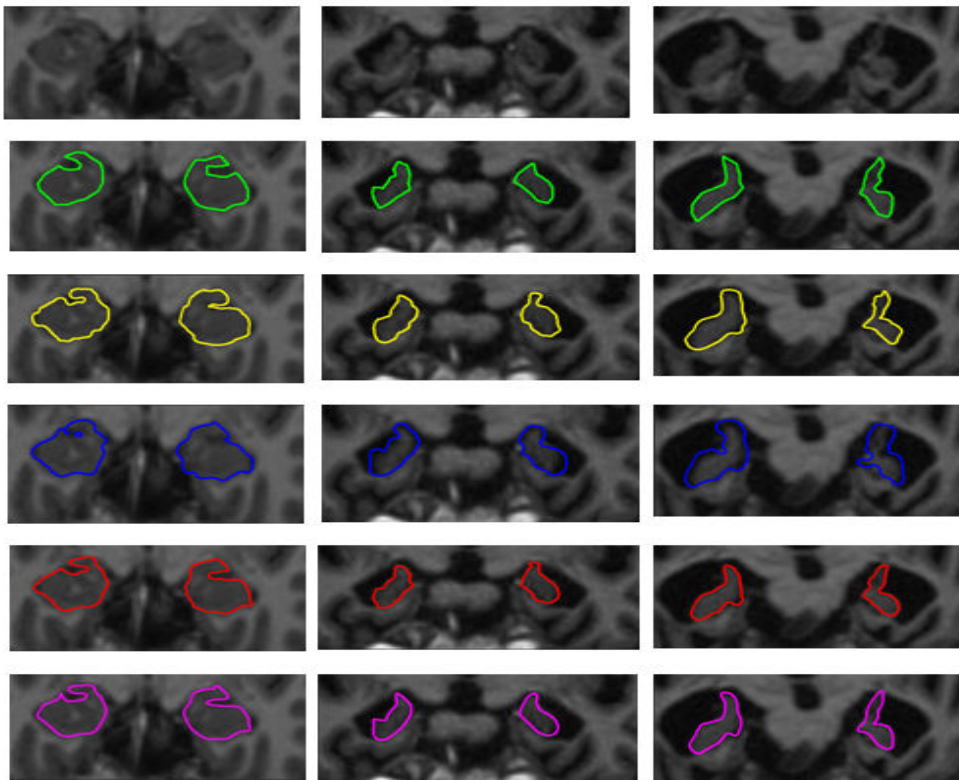


Figure 8. The results of the segmentation of the hippocampus. The six lines present: image zoom on the hippocampus area, manually segmented image, the result of the Caselle method, the result of the Chan&Vese method, the result of the Lankton method, the result of our method. Column 1 shows a healthy subject, column 2 shows a MCI (primary stage) and the third column corresponds to an Alzheimer's subject (advanced stage)

In figure 9 we present a comparison between the manual segmentation, Caselle, Chan&vese, Lankton and our method.

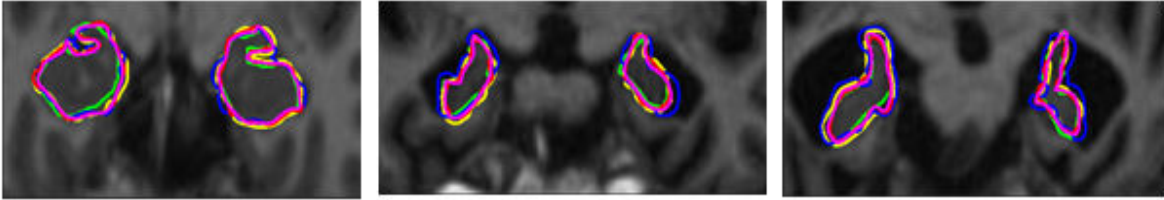


Figure 9. A comparison between the results. Each column shows the superposition of the corresponding results: Caselle (yellow curve), Chan & Vese (blue curve), Lankton (red curve), our method (purple curve), and the ground truth (Green Curve) for a normal subject, MCI and AD

We chose the Hausdorff distances, dice, MSSD (Mean Sum Square Distance) and PSNR (peak signal-to-noise ratio (PSNR)) as a measure of the quality of the segmentation. These metrics are widespread in the medical field and admit multiple applications. In our case, we will use these distances to measure the degree of similarity between two Shapes.

$$PSNR = 10 \log_{10}(\text{Max}^2 | \text{EQMP}) \quad (13)$$

where Max is the maximum peak to peak of the original signal, EQMP is the average of values of EQM_p (weighted mean square error locally on blocks of 8 x 8 pixels).

EQM_p is given by:

$$\text{EQM}_p(I, \hat{I}) = \frac{1}{N^2} \sum_{u=1}^N \sum_{v=1}^N W_{u,v} (I(u, v) - \hat{I}(u, v))^2 \quad (14)$$

I and \hat{I} represent the original images degraded respectively in the DCT domain. $W_{u, v}$ (2) represents the weight of the weighting in the spatial frequency (u, v). N (equal to 8) represents the size of the matrix to which the weighting W is applied.

The dice coefficient is:

$$\text{Dice} = 2 * \text{nnz}(\text{segCont} \& \text{grndTruth}) / (\text{nnz}(\text{segIm}) + \text{nnz}(\text{grndTruth})) \quad (15)$$

where segcont: segment contour; grndTruth: ground truth; nnz: size of the contour

Normal

The figure shows the calculation results of the four distances: Dice, PSNR, Hausdorff and MSS using the four methods (Caselles Chan & Vese, Lankton, our method), compared with the ground truth on three samples.

Normal

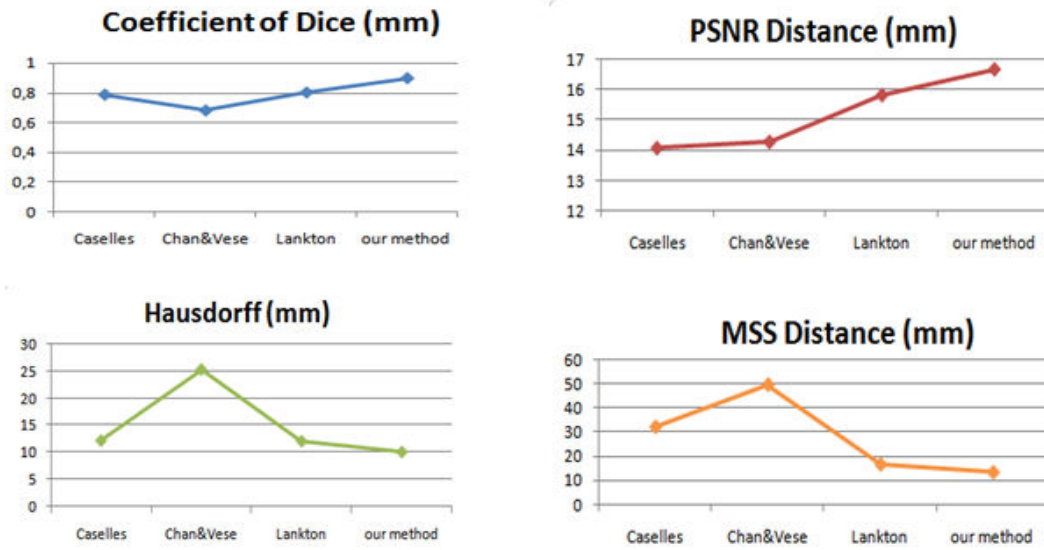


Figure 10. The results of calculating the Hausdorff distances, Dice, PSNR, MSSD between the four methods (Caselles, Chan & Vese, Lanktom, and our method) and the ground truth about a subject Normal following the segmentation of the hippocampus

MCI

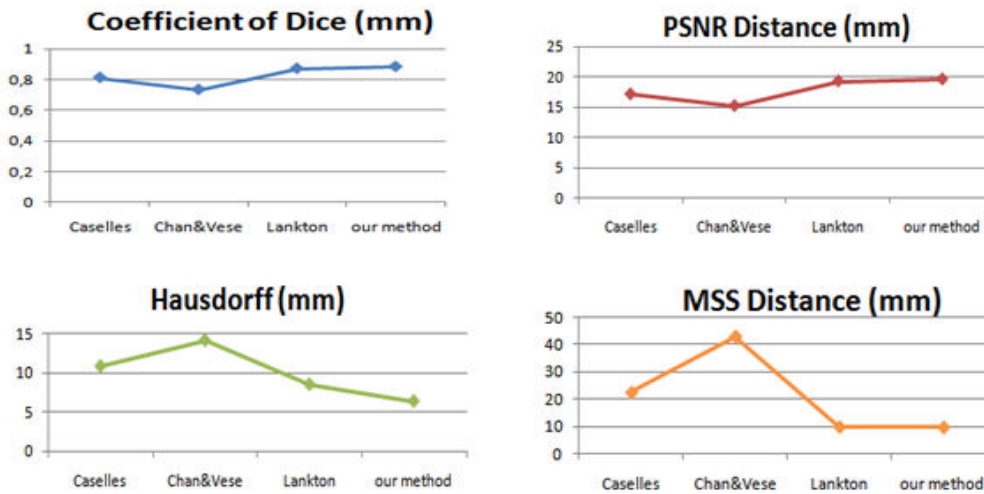


Figure 11. Results of calculating the Hausdorff distances, Dice, PSNR, MSSD between the four methods (Caselles Chan & Vese, Lanktom, our method) .and the ground truth about a MCI subject following segmentation of the hippocampus.

AD

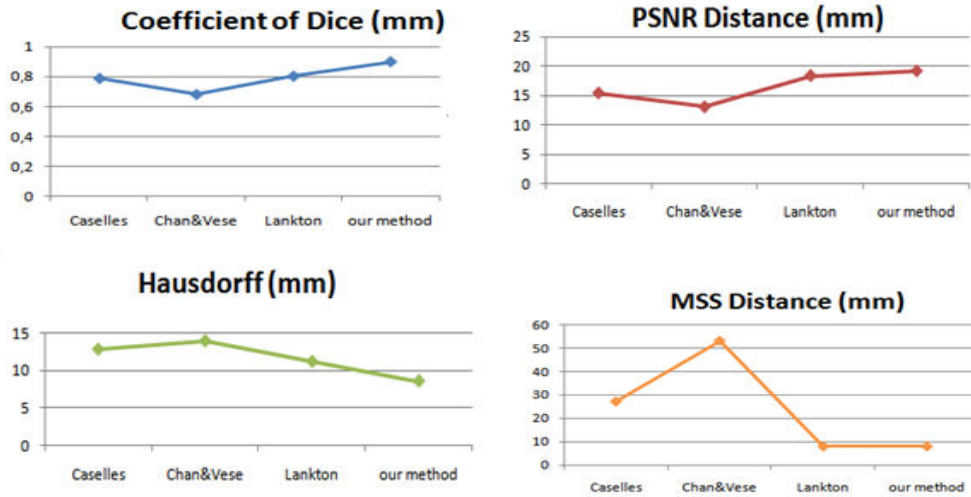


Figure 12. Results of calculating the Hausdorff distances, Dice, PSNR, MSSD between the four methods (Caselles Chan & Vese, Lanktom, our method) .and the ground truth about an AD subject following segmentation of the hippocampus

The result shows the Corpus Calosum segmentation using Caselle, Chan&Vese, Lankton, and our method.

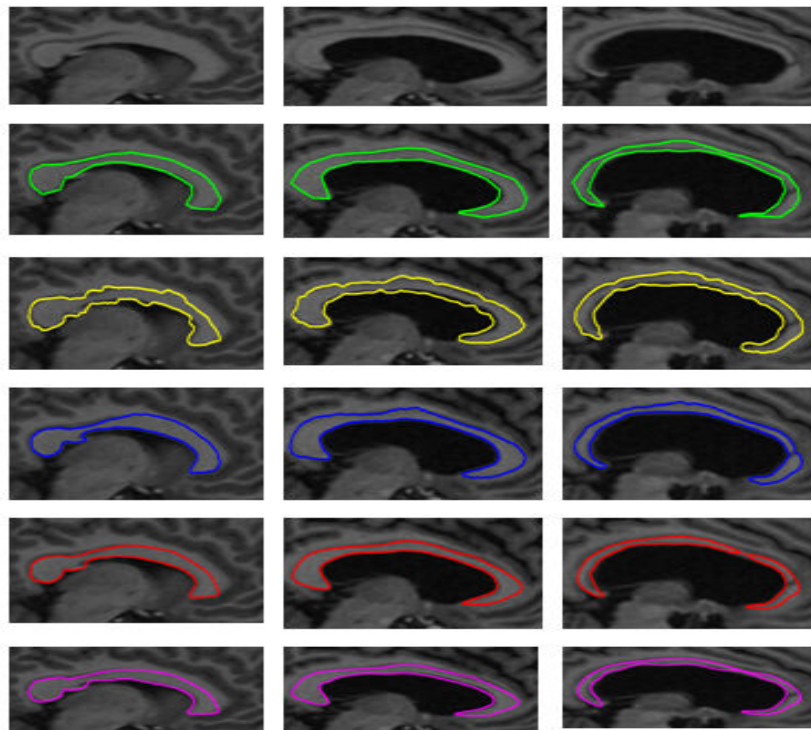


Figure 13. The results of the Corpus Calosum segmentation. The six lines present in order: image zoom on the hippocampus area, manually segmented image, the result of the Caselle method , the result of the Chan&Vese method, the result of the Lankton method, the result of our method. Column 1 shows a healthy subject, column 2 MCI (primary stage), and the third column corresponds to an Alzheimer's subject (advanced stage).

In figure 14, we present in order: the comparison between Caselle, Chan&Vese, Lankton manual segmentation and our method.

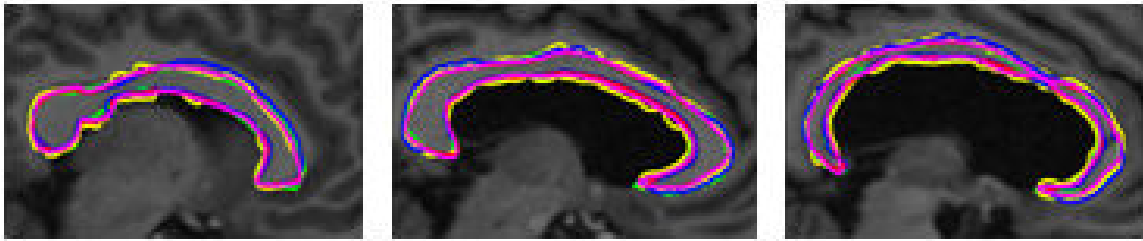


Figure 14. A comparison between the results. Each column shows the superposition of the corresponding results: Caselle (yellow curve), Chan & Vese (curve blue) Lankton (red curve), our method (purple line) and the ground truth (Curve Green) for a normal subject, MCI and AD.

Normal

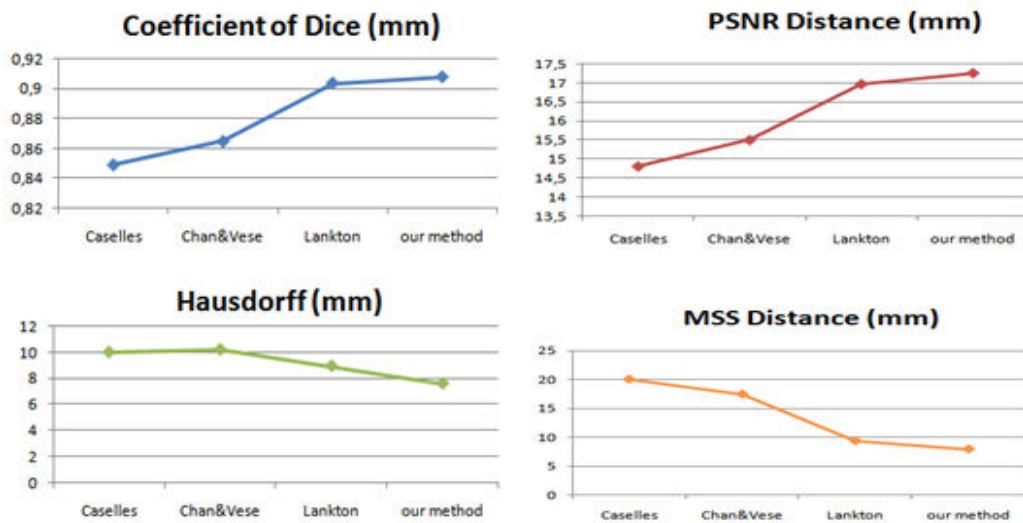


Figure 15. The results of calculating the Hausdorff distances, Dice, PSNR, MSSD for the four methods (Caselles Chan & Vese, Lanktom, our method) and the ground truth about a Normal subject following the Corpus Calosum segmentation.

MCI

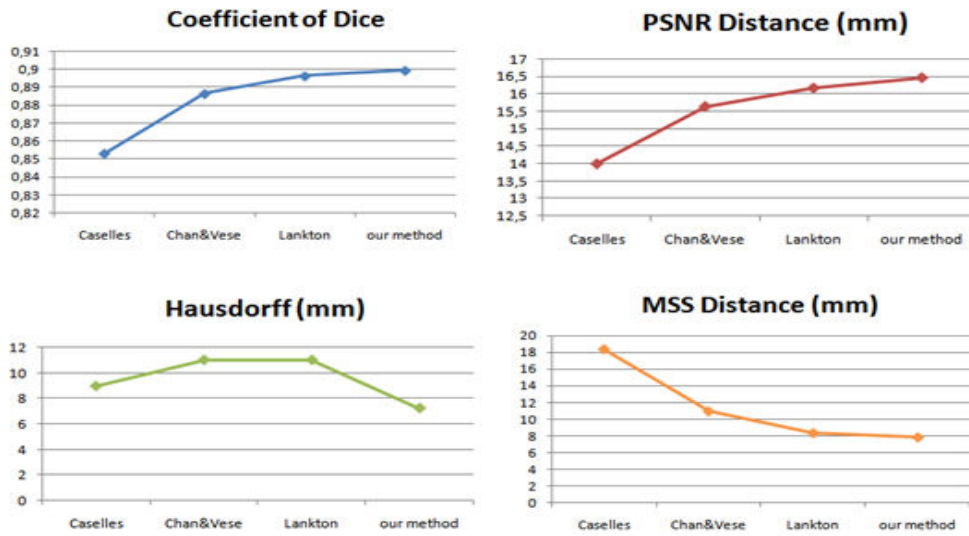


Figure 16. Results of calculating the Hausdorff distances, Dice, PSNR, MSSD between the four methods (Caselles Chan & Vese, Lanktom, our method) and the ground truth about a subject Normal following segmentation of the Corpus Calosum.

AD

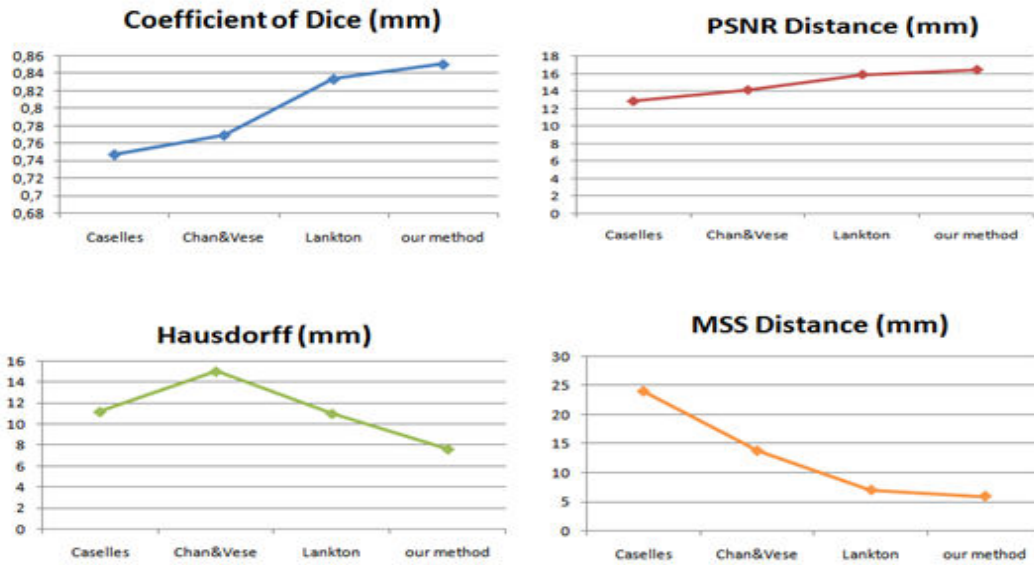


Figure 17. The results of calculating the Hausdorff distances, Dice, PSNR, MSSD for the four methods (Caselles Chan & Vese, Lanktom, our method) and the ground truth about a Normal subject following the Corpus Calosum segmentation.

By examining six diagrams, we can clearly observe that the Green curve which represents the Hausdorff distance has values between 6.34 and 10.16 (mm) for our method of segmentation. On the

contrary, for the other methods, the values of the Hausdorff distance often exhibit large variations, passing from 10.81 (mm) to reach 25.46 (mm).

For the Dice coefficient, our method presents the best values. The values of our method are between 0.885 and 0.918 mm as opposed to the other three methods, whose dice coefficient values vary between 0.681 and 0.873 mm.

For the PSNR coefficient, our method has values between 16.655 and 19.69 mm as opposed to the other methods whose values vary between 14.09 and 18.34 mm.

Yet for the MSSD distance, our method has values between 6.61 and 13.31 mm, while for the other three methods the values are between 9.67 and 47.571 mm.

Through these measures, although in some cases the method of Casselle & Lankton provides acceptable results, we can see that for each sequence our model provides a more stable and comprehensive income closer to the manual segmentation. This can learn about the interests of the integration of priori knowledge.

In conclusion, it is clear that the integration of priori knowledge of the form has greatly improved the results of the image sequences segmentation. That necessarily increases the reliability of the diagnostic parameters which is calculated based on these results.

The classification results

Our database contains 500 subjects and for the evaluation of our method we worked with 75 subjects: 25 Normal, 25 MCI, 25 AD.

	Normal	MCI	AD
Subject	25	25	25

We present three figures representing the accuracy of the classification using the three methods, KNN, SVM and our method for normal, MCI and Alzheimer subjects.

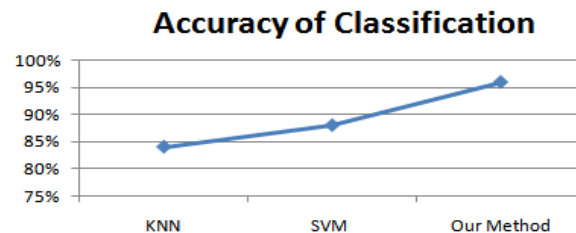


Figure 18. Accuracy of classification using the three methods, KNN, SVM and our method, for normal subjects

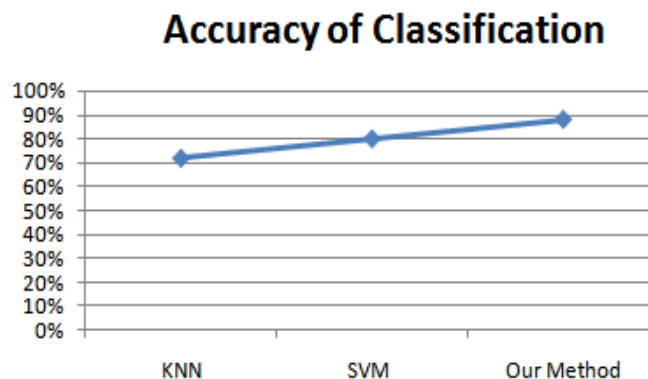


Figure 19. Accuracy of classification using the three methods: KNN, SVM and our method for MCI subjects

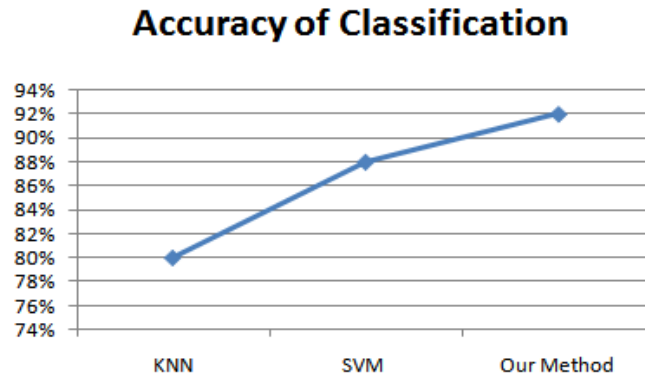


Figure 20. The accuracy of classification using the three methods, KNN, SVM and our method, for AD subjects

Whatever the patient condition, Normal, MCI or AD, our method has provided us with better results. Advocate Example precision for Normal Patients was found 96% as opposed to 88% for the SVM method and 84% for KNN. For MCI patients was found 88% as opposed to 80% for the SVM method and 72% for KNN. Also for AD patients were found 92% as opposed to 88% for the SVM method and 80% for KNN. Our classification method gave us the best results, finding overall accuracy of 92% as opposed to 84% for the SVM method and 78.66% for KNN.

4. Conclusion

We managed to achieve a Computer Assisted Diagnosis system by analyzing the Hippocampus and Corpus Callosum. Our first contribution consisted in presenting a new method of segmentation based on a deformable model and priori knowledge. For the second contribution, we proposed a classification method based on the use of the four known metric distances, and the decision was achieved by using Bayes. We found a good precision of 92% for detecting Alzheimer's disease at any stage. The success of such a system is due to two phases: segmentation and classification. We proposed it as a future work, adding another part to establish the longitudinal monitoring for this disease: the analysis of two MRI of the same patient in two different times for determining the changes in the hippocampus texture descriptors.

5. Acknowledgments

We thank Professor Mouna Ben Djebara from the Alzheimer Service of the Hospital Razi (Tunisia) for kindly providing us brain MRI images and manually segmenting the targeted regions Hippocampus and Corpus Callosum.

References

- Weiner, M.W., Veitch, D.P., Aisen, P.S., Beckett, L.A., Cairns, N.J., Cedarbaum, J. et al. (2015). Impact of the Alzheimer's Disease Neuroimaging Initiative, 2004 to 2014 . *Alzheimers Dement*, 11, pp. 865–884.
- 2015 Alzheimer's disease facts and figures. *Alzheimers Dement*. 11, pp. 332–384.
- Brumfield, M. (2014). The Critical Path Institute: transforming competitors into collaborators. *Nat Rev Drug Discov*, 13: 785–786.

- Neville, J., Kopko, S., Broadbent, S., Aviles, E., Stafford, R., Solinsky, C.M. et al. (2015). Development of a unified clinical trial database for Alzheimer's disease. *Alzheimers Dement*, 11: 1212–1221.
- Romero, K., Sinha, V., Allerheiligen, S., Danhof, M., Pinheiro, J., Kruhlak, N. et al. (2014). Modeling and simulation for medical product development and evaluation: highlights from the FDA-C-Path-ISOP 2013 workshop. *J Pharmacokinet Pharmacodyn*, 41: 545–552.
- Mahad, D. H., Trapp, B. D., & Lassmann, H. (2015). Pathological mechanisms in progressive multiple sclerosis. *Lancet Neurol*, 14: 183–193.
- Geerts, H., Roberts, P., Spiros, A., & Potkin, S. (2015). Understanding responder neurobiology in schizophrenia using a quantitative systems pharmacology model: Application to iloperidone. *J Psychopharmacol*, 29: 372–382.
- Kuffner, R., Zach, N., Norel, R., Hawe, J., Schoenfeld, D., Wang, L. et al. (2015). Crowdsourced analysis of clinical trial data to predict amyotrophic lateral sclerosis progression. *Nat Biotechnol*, 33: 51–57.
- Ruan, L., Lau, B.W., Wang, J., Huang, L., Zhuge, Q., Wang, B. et al. (2014). Neurogenesis in neurological and psychiatric diseases and brain injury: from bench to bedside. *Prog Neurobiol*, 115: 116–137.
- Cummings, J.L., Morstorf, T., & Zhong, K., (2014). Alzheimer's disease drug-development pipeline: few candidates, frequent failures. *Alzheimers Res Ther*, 6:p. 37.
- Romero, K., Ito, K., Rogers, J.A., Polhamus, D., Qiu, R., Stephenson, D. et al. (2015). The future is now: model-based clinical trial design for Alzheimer's disease *Clin Pharmacol Ther*, 97, pp. 210–214.
- Panza, F., Solfrizzi, V., Imbimbo, B.P., Tortelli, R., Santamato, A., & Logroscino, G. (2014). Amyloid-based immunotherapy for Alzheimer's disease in the time of prevention trials: the way forward *Expert Rev Clin Immunol*, 10, pp. 405–419.
- Saykin, A.J., Shen, L., Yao, X., Kim, S., Nho, K., Risacher, S.L. et al. (2015). Genetic studies of quantitative MCI and AD phenotypes in ADNI: Progress, opportunities, and plans *Alzheimers Dement*, 11, pp. 792–814.
- Collins, F. S. & Varmus, H. A. (2015). New initiative on precision medicine *N Engl J Med*, 372, pp. 793–795.
- Hartley, S. L., Handen, B. L., Devenny, D. A., Hardison, R., Mihaila, I., Price, J. C. et al. (2014). Cognitive functioning in relation to brain amyloid-beta in healthy adults with Down syndrome *Brain*, 137, pp. 2556–2563.
- Aljabar, P., Heckemann, R.A., Hammers, A., Hajnal, J.V., & Rueckert, D. (2009). Multi-atlas based segmentation of brain images: atlas selection and its effect on accuracy. *Neuroimage*, 46:726–738.
- Atif, J., Nempont, O., Colliot, O., Angelini E., & Bloch. I. (2006). Level Set Deformable Models Constrained by Fuzzy Spatial Relations. In *Information Processing and Management of Uncertainty in Knowledge-Based Systems*, IPMU, pp. 1534–1541, France.
- Ardekani, B. A. & Bachman. A. H. (2009). Model-based automatic detection of the anterior and posterior commissures on MRI scans. *Neuroimage*, 46:677–682 .
- Delingette, H. & Montagnat, J. (2001). Shape and topology constraints on parametric active contours. *Computer Vision Image Understanding*, vol.83, pp. 140-171.
- Duvernoy, H. M. (2005). *The Human Hippocampus: Functional Anatomy, Vascularization and Serial Sections with MRI*. Springer.
- Andreopoulos, A. & Tsotsos, J. (2008). Efficient and generalizable statistical models of shape and appearance for analysis of cardiac MRI. *Medical Image Analysis*, pp. 335-357.
- Aymeric, H. & Christine, C. M. (2005). Détection robuste et automatique des contours myocardiques sur des séquences IRM cardiaques marquées.

- Babalola, K. O., Patenaude, B., Aljabar, P., Schnabel, J., Kennedy, D., Crum, W., Smith, S., Cootes, T., Jenkinson, M., & Rueckert, D. (2009). An evaluation of structures in the brain. *NeuroImage*, Vol. 47, pp. 1435-1447.
- Bascle, B. (1994). Contributions et applications des modèles déformables en vision par ordinateur. Thèse de doctorat, université de Nice-sophia antipolis.
2008. Segmentation des tissus et structures sur les IRM cérébrales : agents markoviens locaux coopératifs et formulation bayésienne. Thèse de doctorat, Institut National Polytechnique de Grenoble.
- Caselles, L., Catt, F., Coll, C., & Dibos, F. (1991). A geometric model for active contours in image processing. *Numerische Mathematik*, pp. 1-3.
- Caselles, V., Kimmel, R., & Sapiro, G. (1997). Geodesic Active Contours. *International Journal of Computer Vision*, vol.22, pp. 61-79.
- Chan, T. & Vese, L. (2001). Active contours without edges. *IEEE Trans. on Image Processing*, vol.10, pp. 266-277.
- Charmi, M. A., Derrode, S., & Ghorbel, F. (2008). Fourier-based geometric shape prior for snakes. *Pattern Recognition Letters*, vol.29, pp. 897-904.
- Chen, C. H. & Lee, G. G. (1997). Image Segmentation Using Multiresolution Wavelet Analysis and Expectation-Maximization (EM) Algorithm for Digital Mammography. *International Journal of Imaging Systems and Technology*, Vol.8, pp. 491-504.
- Chen, W. & Giger, M. L. (2004). A fuzzy c-means (FCM) based algorithm for intensity inhomogeneity correction and segmentation of MR images. *IEEE International Symposium on Biomedical Imaging*, Arlington, VA, pp.1307-1310.
- Chen, S. & Radke, R. J. (2009). Level set segmentation with both shape and intensity priors. *12th IEEE International Conference on Computer Vision*, pp.763 -770.
- Cohen, L. D. (1991). On Active contour models and balloons. *CVGIP: Image Understanding*, vol.53, pp. 211–218.
- Cootes, T. F. & Taylor, C. J. (1994). Combining point distribution models with shape models based on finite element analysis. *BMVC94: Proceedings of the conference on British machine vision*, vol.2, pp. 419-428.
- Cootes, T. F., Taylor, C. J., Cooper, D. H., & Graham, J. (1995). Active Shape Models - Their Training and Application. *Computer Vision and Image Understanding*, vol. 61, pp. 38-59.
- Cootes, T. F., Edwards, G. J., & Taylor, C. J. (2001). Active Appearance Models. *IEEE Trans. Pattern Anal. Mach. Intell.*, vol.23, pp. 681-685.
- Cootes, T. F. & Taylor, C. J. (1994). Combining point distribution models with shape models based on finite element analysis. *BMVC94: Proceedings of the conference on British machine vision*, vol.2, pp. 419-428.
- Caselles, V., Kimmel, R., & Sapiro, G. (1997). Geodesic Active Contours, *International Journal of Computer Vision* .
- Chan, T. & Vese, L. (2001). Active Contours without Edges, *IEEE Transactions on Image Processing*.
- Lankton, S. & Tannenbaum, A. (2008). Localizing region-based active contours, *IEEE Transaction on Image Processing*.
- Cover, T. & Hart, P.E. (1967). Nearest neighbor pattern classification. *IEE Transactions Information Theory*, 13:21–27.
- Quinlan, J. (1986). Induction of decision trees. *Machine Learning*, 1(1):81–106.
- Cortes, C. & Vapnik, V. (1995). Support-vector networks. *Machine learning*, 20(3) :273–297.
- Sahiner, B., Petrick, N., Chan, H-P., Hadjiiski, L.M., Paramagul, C., Helvie, M. A. et al. (2001). Computer-aided characterization of mammographic masses: accuracy of mass segmentation and its effects on characterization. *IEEE Trans Med Imaging*, 20:1275–84.

- Huttenlocher, D. P., Klanderman, G. A., & Rucklidge, W. J. (1993). Comparing images using the Hausdorff distance. *IEEE Trans Pattern Anal Mach Intell*, 15:850–63.
- Hooper, M. (2013). « Richard Price, Bayes ' theorem, and God », *Significance*, vol. 10, no 1, février.